IFSCC 2025 full paper (IFSCC2025-751)

"Virtual Screening of Kelch-like ECH-Associated Protein 1−Nuclear Factor Erythroid 2‑Related Factor 2 (Keap1−Nrf2) In-hibitors and In Vitro Validation"

Zhengwan Huang 1, Zhengang Peng [1,*], Dandan Huang 1 and Zhongyu Zhou [2,*]

[1] Bloomage Biotechnology Corporation Ltd.; [2] Guangdong Provincial Key Laboratory of Applied Botany & Key Laboratory of National Forestry and Grassland Administration on Plant Conservation and Utilization in Southern China, South China Botanical Garden, Guangzhou, China

1. Introduction

Ultraviolet B (UVB) radiation is known to induce the generation of reactive oxy-gen species (ROS), including superoxide anion ($\cdot O^{2-}$), hydroxyl radical ($\cdot OH$), hydrogen peroxide (H_2O_2) and singlet oxygen ($^1O_2$) [1, 2]. The excessive accumulation of ROS leads to direct deleterious chemical modifications of cellular components, such as DNA, lipids, and proteins [3, 4]. Furthermore, ROS contribute to the degradation of collagen by inducing the upregulation of matrix metalloproteinase (MMP) activity, which breaks down the extracellular matrix and impairs skin integrity and elasticity [5]. Both the chemical oxidation of cellular components and the activation of cellular machinery, brought about by ROS, act in concert to cause aging [6, 7]. The transcription factor nuclear factor erythroid 2-related factor 2 (Nrf2) promotes the production of approximately 250 antioxidant proteins, including heme oxygenase-1 (HO-1), NAD(P)H quinone oxidoreductase 1 (NQO1), superoxide dismutase (SOD), glutathione S-transferase (GST), and thioredoxin reductase (TRx). It is considered to suppress reactive oxygen species (ROS) production and ROS-related inflammation [8]. In a non-stress situation, the Nrf2-ECH homology 2 (Neh2) domain of Nrf2 is bound by two molecules of the adapter protein Keap1. The two Keap1 molecules form a homodimer via their BTB domains, which also form the binding site for Cullin3 (CUL3), bringing Nrf2 into proximity to the CUL3-Really interesting new gene (RING)-box 1 (RBX1) E3 ubiquitin ligase complex. The level of Nrf2 is kept low post translationally through the action of the ubiquitin proteasome system [9].

When cells are exposed to oxidative or xenobiotic stress, the Keap1-Nrf2 complex dissociates and the ubiquitylation of Nrf2 is blocked, and Nrf2 translocates into the nucleus, and dimerizes with another bZip transcription factor, one of the small musculoaponeurotic fibrosarcoma (sMAF) proteins. This heterodimer binds the antioxidant response elements (AREs) and ARE-regulated genes (antioxidant genes and anti-inflammatory factors such as HO-1 and NQO1) are activated to enhance cellular defense. The antioxidant and anti-inflammatory effects of the Nrf2 pathway are regarded as beneficial for anti-aging treatments [10].

The Keap1 protein is the best studied and the most critical Nrf2 negative regulator, utilizing both covalent and non-covalent strategies. The covalent modification of reactive cysteines has

been clinically validated as a feasible approach [11], which includes the identification of dimethyl fumarate and sulforaphane [11-12]. Nevertheless, these compounds likely modify other cysteines in the proteome leading to potential toxicity, there is a growing interest in the discovery and development through non-covalent strategies leading to the direct inhibition of the Keap1-Nrf2 protein-protein interac-tion (PPI). The non-covalent Keap1 inhibitors are expected to offer higher target selec-tivity and enhanced safety compared to covalent inhibitors [13].
Natural products and traditional Chinese medicine are widely utilized in the treatment of various illnesses, as documented in pharmacopoeias. Natural compounds like curcumin[14] and lycopene[15] have been identified as potent Nrf2 agonists. This suggests that natural Nrf2 agonists may be employed as chemopreventive and chemo-therapeutic agents for anti-aging applications in skincare products.
Virtual screening is a Computer-Aided Drug Discovery (CADD) method used to identify potential candidates from a silicon database. Compared to in vitro screening, virtual screening significantly reduces both costs and time. This method can be broadly categorized into two groups: 'structure-based' and 'ligand-based' virtual screening, depending on the pharmacophore utilized for model construction [16, 17]. In this context, ligand-based molecular docking is employed to screen for inhibitors of Keap1-Nrf2 from natural compounds.

2. Materials and Methods

2.1. Experimental procedure

Figure 1 shows the workflow utilized in this report.

2.2. Materials

2.2.1. reagents and materials

Acetonitrile (ACN), ethanol (EtOH) and methanol (MeOH) were HPLC grade and purchased from Sigma Aldrich (Milan, Italy). Formic acid (FA) was HPLC grade and purchased from Shanghai Anpel Experimental Technology Co. Ltd. (Shanghai, China). Sodium chloride (NaCl) was purchased from Sinopharm Chemical Reagent Co. Ltd. (Shanghai, China). Milli-Q water was obtained in-house using a Millipore system (Bedford, MA, USA). Chebulinic acid, tubuloside B, angoroside C, epmedin C, senno-side B, cinnamtannin B-1, 6‴-Feruloylspinosin, forsythiaside A and rabdosiin were purchased from Topscience Co. Ltd. (Shanghai, China). Silk protein (BNA-F-F, contains 0.5 % fibroin, and 5 % pentylene glycol 94.5 % water) was purchased from Sinate Bio-technology Co. (Suzhou, China).

2.2.2. Software for molecular docking and visualization

AutoDock Vina version 4.2.6 was employed for docking simulations [18]. The interactions between the ligand-protein complexes were visualized using PyMol version 1.1.7 and the PLIP online server (https://plip-tool.biotec.tu-dresden.de/).

2.3. Model construction for molecular docking

2.3.1. Protein Preparation

Three-dimensional coordinates of Keap1 (PDB code 8IXS) were retrieved from the Protein Data Bank (http://www.rcsb.org) [9]. The PDB file was examined for missing side chains and subsequently processed using AutoDockTools(ADT version 1.5.6) to prepare the PDBQT file. During this process, water molecules and ions were removed, only polar hydrogens were retained, and Gasteiger charges were computed for the protein atoms using ADT.

2.3.2. Ligands Preparation

A database of natural compounds containing over 16,000 entries from TSbitochem (www.tsbioche m.com) was utilized for virtual screening. All the molecules in the database were automatically converted to PDBQT format using OpenBabel (version 3.1.1).

2.3.3. Docking procedure

The 3D structures of the target proteins, provided in .pdb format, were obtained from the Protein Data Bank (PDB) database (https://www.rcsb.org/). AutoDock Vina was utilized for docking to ascertain the optimal conformation. The docking pocket was delineated based on the original ligand's position within the target protein complex. Following the docking process, the interactions between the active compounds and target proteins were analyzed using PyMOL, which also generated the complex .pdb file for further investigation of the interactions between the ligand and protein via PLIP. The key amino acids essential for the screening model were identified based on the docking data of ten inhibitors from ChEMBL.

2.4. Cell-based assays

2.4.1 Cell Culture and H_2O_2 Treatment

Human epithelial keratinocyte (HaCaT) cells were obtained from Sunncell Biotechnology Co., Ltd. (Wuhan, Hubei Province, China). The HaCaT cells were cultured in a humidified atmosphere containing 5% CO_2 at 37°C in Dulbecco's Modified Eagle's Medium (DMEM; Gibco, Cat. No. 11965092), supplemented with 10% fetal bovine serum (FBS; Gibco, Cat. No. 10091148) and 1% penicillin/streptomycin (P/S; Gibco, Cat. No. 15140122). Subsequently, the HaCaT cells were co-treated with candidate compounds and H_2O_2 (100 μM) and incubated for 24 hours.

2.4.2. RNA Extraction and RT-qPCR

Total RNA was extracted using the RNeasy Mini Kit (Qiagen, Hilden, Germany) following the manufacturer's instructions. The extracted RNA was quantified using the Synergy H1 (BioTek, MA, USA). Subsequently, the RNA was reverse transcribed into complementary DNA (cDNA) using the PrimeScript™ RT reagent kit (Takara, Shiga, Japan). The expression of Nrf2 was assessed using SYBR Premix Ex Taq II (Takara, Shiga, Japan) with the forward primer 5'-ACAATGAGGTTTCTTCGGCTAC-3' and the reverse primer 5'-CGTCTAAATCAACAGGGGCTAC-3'. All quantitative PCR (qPCR) analyses were conducted with the QuantStudio 3 Real-Time PCR Instrument (Thermo Scientific, MA, USA). The relative expression level of the target gene was calculated using the ddCt method, with GAPDH serving as the internal control.

2.5. Bioavailability study for the candidate inhibitor

2.5.1. Silk protein encapsulation technology

In order to applicate in cosmetics, the active molecules should be penetrated into the stratum corneum of skin. Actives from nature extract has the drawback that not easy penetrate the stratum corneum of skin, in this situation, actives delivered technologies could be applied to help the actives penetrate into the stratum cornrum including nanocream, lipsome and so on. In this experiment, silk protein encapsulation technology was applied[19]. The selected candidate substances with silk protein encapsulation were compared to those without silk protein encapsulation.

A mixture of 5 g diethylene glycol monoethyl ether (DEGME) and 5.4 g pure water was combined with 0.1 g of chebulinic acid powder to form phase A. This phase was stirred and dissolved until it became transparent and uniform. Concurrently, 14.5 g of butanediol and 25 g of BNA-F-F were mixed uniformly to create phase B. Subsequently, phase A was added dropwise to phase B at room temperature while maintaining constant stirring for 0.5 hour to ensure the complete loading of chebulinic acid onto the silk fibroin. Finally, after 5 minutes of homogenization at 7000 rpm through T 25 digital ULTRA-TURRAX® (IKA, Germany), the silk fibroin encapsulated chebulinic acid was obtained..

2.5.2. Franz Diffusion Cell (FDC)

Franz diffusion cells (FDC; Phoenix DB-6, Hanson) with 0.33 cm^2 diffusion surface and 7.0 mL receptor volume were employed. Reconstructed human epidermis (RHE) samples were preconditioned with isotonic phosphate-buffered saline (PBS, pH 7.4) and positioned between the

donor and receptor chambers with the stratum corneum layer oriented upward. The receptor compartment received 7.0 mL PBS (37°C) degassed via sonication to eliminate microbubbles at the membrane-solution interface.
The experimental design comprised: Test group: 0.2 mL chebulinic acid (1% w/v) encapsulated in silk fibroin matrix (n=3); Control group: 0.2 mL free chebulinic acid solution (1% w/v, n=3).
The system was maintained at 37±0.5°C via thermostatically controlled water jacket. Receptor medium was continuously agitated at 600 rpm using a Teflon-coated magnetic stir bar (Ø5×10 mm) to maintain sink conditions. Independent triplicate experiments were conducted with fresh RHE specimens for each trial.
At 24-hour intervals, cells were harvested from the temperature-controlled incubator, and the collected samples (n=3 per time point) were analyzed in triplicate using ultra-high-performance liquid chromatography (UHPLC) to quantify chebulinic acid levels.
2.5.3. UHPLC-MS
Liquid chromatographic separation was achieved using a Welch Xtimate UHPLC C18 column (2.1 x 100 mm, 1.8 μm particle size) at a flow rate of 300 μL/min. Composition of mobile phases A and B were water with 0.1% formic acid, and methanol with 0.1% formic acid, respectively. The eluent gradient was: 10% B for 2 min, then the eluent from 10% B to 90% B in 4 min, kept for 2 min, then from 90% B to 10% B in 2 min, kept for 2 min.
A Q-Exactive hybrid Quadrupole-Orbitrap mass spectrometer (Thermo Fisher Scientific) was used for high resolution qualitative analysis of chebulinic acid. The mass spectrometer was operated in electrospray negative mode. Full scan and targeted MS/MS analysis was acquired at m/z 100-1500 Da. Other mass spectrum parameters are referred to the literature[20]..

3. Results and discussion

3.1. Molecular Docking Screening Model Construction

Seven Keap1 commercial inhibitors from ChEMBL database were selected to establish the molecular docking screening model of Keap1 inhibition. These seven inhibitors are listed in the database as ChEMBL3601212, ChEMBL3899754, ChEMBL4174651, ChEMBL4544116, ChEMBL4646536, ChEMBL4757197, and ChEMBL4762197, which showed half-maximal inhibitory concentration values (IC50) ranged from 0.14 to 120 nmol/L.
The docking results (Table 1) showed that all the 7 inhibitors had good binding affinity with Keap1 (with binding energies below -9 kcal/mol indicating strong binding interactions [21]).
From Table 1, it was found that Tyr334, Arg483, Arg415, Tyr525, and Ala556 were most frequent residual of Keap1 interacted with seven inhibitors. The interactions between the inhibitor and Keap1 were shown in Fig 2. The interaction analysis by PLIP (Protein-Ligand Interaction Profiler) showed that the inhibitor interacted with those residuals of Keap1 in the forms of hydrogen bond, pi-cation interactions and hydrophobic interactions, which indicated that the interactions between inhibitors and Keap1 were non-covalent rather than covalent with the Cys151 of Keap1 [22]. Based on the established model, we propose that the Keap1 inhibitors selected for virtual screening must meet two criteria: First, the binding energy should be less than -9 kcal/mol. Second, the interacting residues with Keap1 must include at least four of the following five amino acid residues: Tyr334, Arg483, Arg415, Tyr525, and Ala556. Furthermore, considering the research and development costs, the price of the virtual Keap1 inhibitors should be limited to 400 yuan per milligram.

3.2. Virtual Screening of Keap1 Inhibitors

Our investigation evaluated around 16,000 natural compounds for their potential as Keap1 inhibitors, with a focus on disrupting the Keap1-Nrf2 protein-protein interaction (PPI). According to the virtual screening model for the inhibitors searching in the database, nine of these

compounds were proposed as the candidate inhibitors that exhibited high binding energy and engaged with at least four amino acid residues. The nine compounds were chebulinic acid, tubuloside B, angoroside C, epmedin C, sennoside B, cinnamtannin B-1, 6‴-feruloylspinosin, forsythiaside A and rabdosiin. The chemical structures of these compounds are depicted in Fig 3. The binding energy and interacted amino acid residuals were recorded in Table 2.

3.3. Validate the predict results by in vitro experiment

3.3.1. Six candidates stimulated the Nrf2 expression in HaCaT cells

To validate the virtual screening results, the nine candidates were tested in the model constructed in HaCaT cells that stimulated with H_2O_2 to mimic the oxidative stress. From Fig 4, the mRNA expression of Nrf2 is significant decreased under oxidative stress of H_2O_2. S10 is a commercial agonist of Nrf2 as well as inhibitor of Keap1-Nrf2, in this validation experiment, it was used as positive control. It exhibited promising ability to promote the mRNA expression of Nrf2, which indicated that this screening model is effective. Six of these nine compounds including chebulinic acid, epmedin C, 6‴-feruloylspinosin, forsythiaside A, cinnamtannin B-1 and rabdosiin exhibited promising ability to promote the mRNA expression of Nrf2, the promotion rate ranging from 23% to 50% compared with control group (Figure 4).

Among the 6 candidates, chebulinic acid showed the highest increasing of mRNA expression of Nrf2 to combat with oxidative stress. Not all compounds can effectively penetrate the stratum corneum. For cosmetics to function optimally, their active ingre-dients must be able to permeate this layer. To conduct a more comprehensive assess-ment of the potential applications of chebulinc acid in both the pharmaceutical and cosmetics industries, a penetration study has been performed.2.5. Validating the Predicted Results by In Vitro Experiment

3.4. Penetration studying

The content of chebulinic acid in the sample encapsulated in silk fibroin was determined to be 2000 mg/L through liquid ultra-high performance liquid chromatography-mass spectrometry (UHPLC-MS). According to the Fig 5 it was found that chebulinic acid could not penetrate into the corneum alone, while with the help of delivered technology, the bioavailability was greatly enhanced. This indicated that it could be applied as inhibitor of Keap1-Nrf2 to combat with oxidative stress in cosmetics industry. It also showed that virtual screening model with delivered technology could be an effective solution to screen active compounds in cosmetics industry.

1.1. Figures, Tables and Schemes

Table 1. Residuals involved in the interaction between seven commercial inhibitors and Keap1

ChEMBL ID	IC50 (nM)	Binding energy (kcal/mol)	Residual
3899754	0.14	-11.6	Phe557, Tyr334, Ser363, Arg415, ALa556, Ser508, Phe478, Arg483
3601212	14.40	-9.3	Arg483, Tyr525, Ser555, Ala556, Arg415, Tyr334, Ser363, Asn382
4544116	15.80	-10.4	Arg483, Tyr525, Gln530, Phe478, Asn414, Ala556, Ser602, Asn382
4757197	48.00	-9.4	Tyr572, Gln530, Ile559, Val512, Tyr525, Arg415, Arg483, Ile461, Phe478
4174651	60.00	-9.7	Asn382, Asn414, Ser363, Arg415, Tyr334, Ser602, Ala556, Ser555, Tyr525, Ser508, Arg483
4646536	73.00	-9.2	Ser508, Tyr525, Ser555, Ala556, Tyr334, Ser363, Arg415

4762197	120.00	-10.4	Ser363, Asn382, Tyr334, Arg415, Ala556, Phe577, Gln530

Table 2. Binding energy and interactive residuals involved in the interaction between nine inhibitors and Keap1

Compound	Binding energy (kcal/mol)	Residuals	
		Hydrogen bonding	Hydrophobic interactions
Chebulinic acid	-10.4	Ser363, Asn382, Asn414, Arg415, Ile461, Arg483, Tyr525, Gln530, Ser602	Tyr334, Tyr525, Ala556
Angoroside C	-10.3	Arg415, Arg483, Tyr525, Ser555, Ser602	Tyr334, Arg415, Ala556
Sennoside B	-10.1	Ser363, Asn382, Val418, Ile461, Val465, Ser508, Gly509, Val512, Tyr525, Gln530, Leu557, Ser602	Tyr334, Arg415, Phe478, Tyr525, Ala556
Tubuloside B	-9.9	Ser363, Asn382, Ile416, Val463, Arg483, Ser508, Gln530, Ser602, Tyr334, Arg415	Tyr525, Ala556
Epmedin C	-9.8	Arg483, Tyr525, Gln530, Ser555, Leu557	Tyr334, Arg415, Ala556, Tyr572
Rabdosiin	-9.7	Ser363, Asn382, Gly462, Arg483, Ser508, Tyr525, Gln530, Tyr572, Ser602	Tyr334, Arg415, Tyr525, Ala556, Tyr572, Phe577
6‴-Feruloylspinosin	-9.3	Ser363, Asn382, Asn414, Arg415, Arg483, Ser508, Tyr525, Gln530, Ser555, Ser602	Tyr334, Arg415, Tyr525, Ala556
Forsythiaside A	-9.2	Ser363, Gly364, Asn382, Arg415, Arg483, Ser508, Ala510, Gln530, Ala556	Tyr334, Tyr525, Ala556
Cinnamtannin B-1	-9.2	Tyr334, Arg415, Arg483, Gly509, Tyr525, Gln530, Tyr572	Tyr334, Tyr525, Ala556

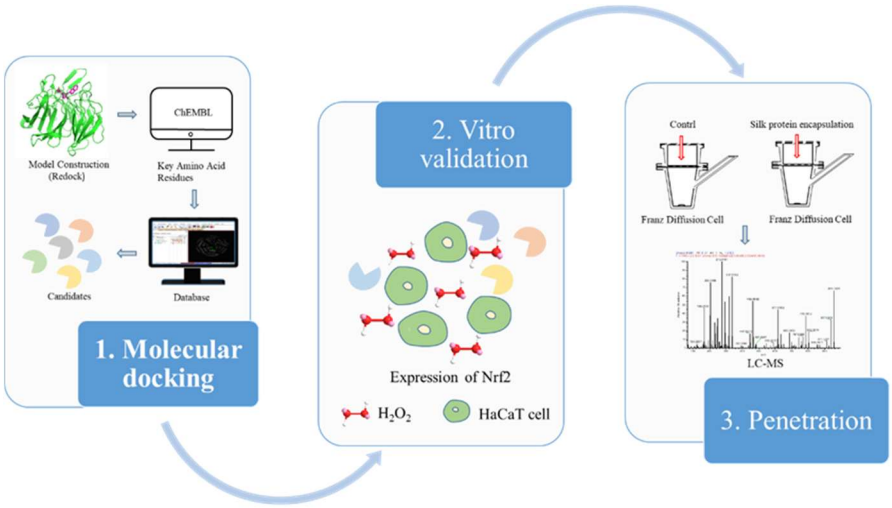

Figure 1. Flow chart of the experimental procedure.

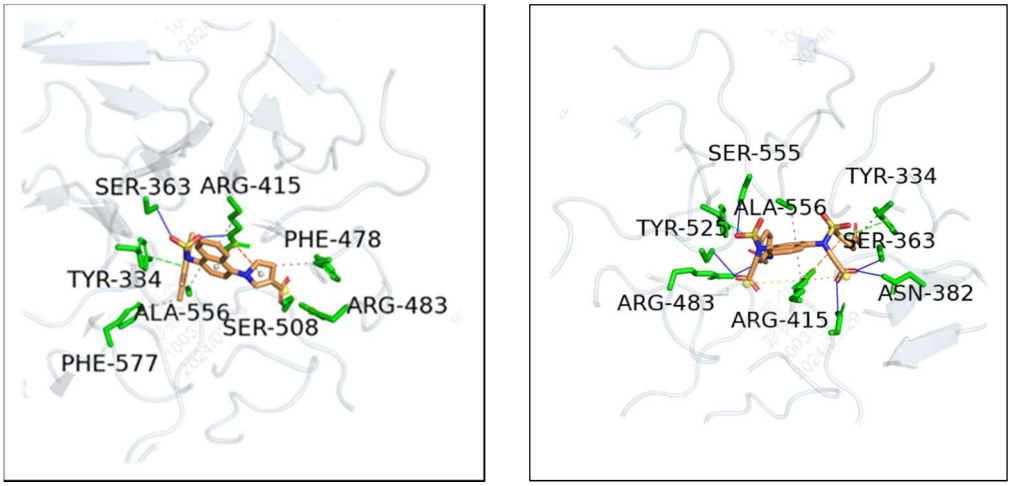

Figure 2. Binding of 3899754 (left) and 3601212 (right) into the active site of Keap1.

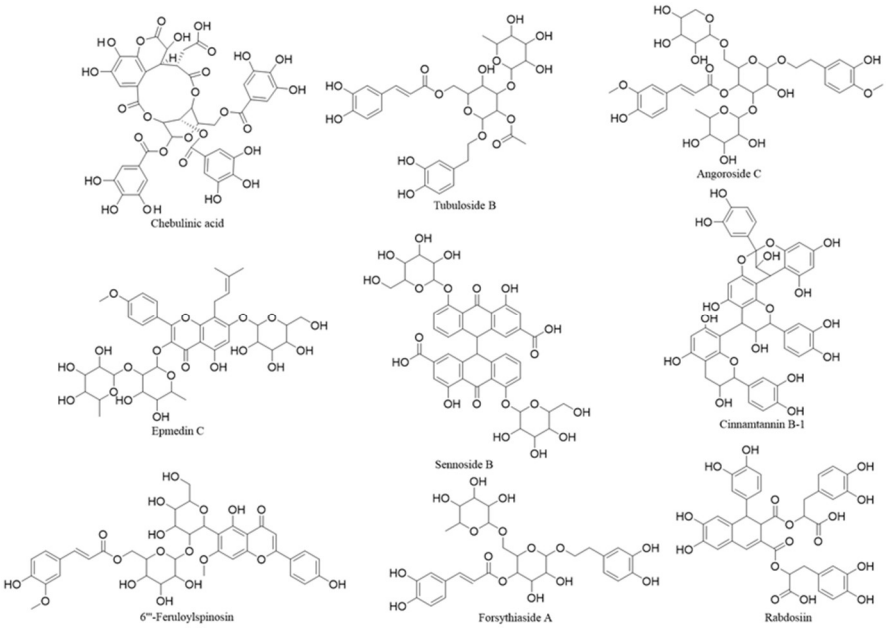

Figure 3. Nine Keap1 inhibitors identified by virtual screening.

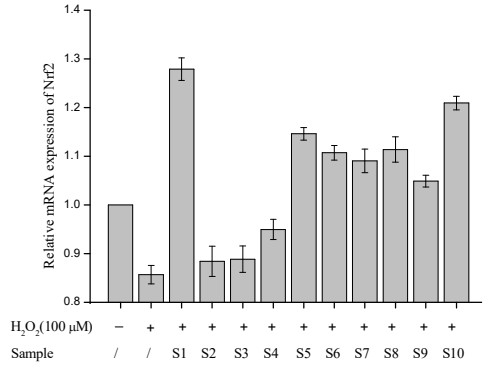

Figure 4. Relative mRNA expression of Nrf2 was quantified in HaCaT cells via RT−qPCR. Results are expressed as means ± SDs of three independent experiments. S1：chebulinic

acid. S2: angoroside C. S3: angoroside C. S4: tubuloside B. S5: epmedin C. S6: rabdosiin. S7: 6‴-feruloylspinosin. S8: forsythiaside A. S9: cinnamtannin B-1. S10: RA 839.

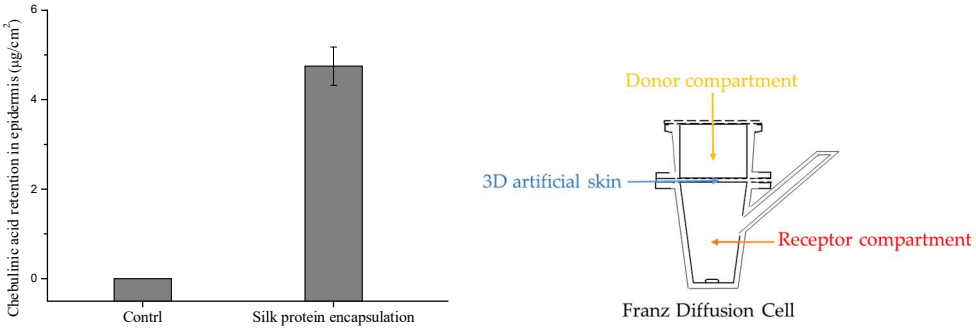

(a) (b)

Figure 5. (a) Chebulinic acid recovery from the skin and receptor liquid after the application of silk protein encapsulation after 24 h (mean ± SD, n = 3); (b) Franz diffusion cell.

4. Conclusion

A virtual screening model for the direct non-covalent inhibition of the Keap1-Nrf2 protein-protein interaction was successfully established, utilizing molecular docking technology. Our selection criteria, which included a binding energy threshold of less than -9 kcal/mol and interactions with 4-5 key amino acid residues, were corroborated by seven commercial Keap1 inhibitors.

Applying this virtual screening model, nine natural compounds were selected, including chebulinic acid, tubuloside B, angoroside C, epmedin C, sennoside B, cinnamtannin B-1, 6‴-Feruloylspinosin, forsythiaside A, and rabdosiin. These candidates engaged with the Keap1 residues via hydrogen bonds, pi-cation interactions and hydrophobic interactions.

Cell-based assays validated the effectiveness of nine selected compounds. Among six in nine, namely chebulinic acid, epmedin C, 6‴-feruloylspinosin, forsythiaside A, cinnamtannin B-1, and rabdosiin, significantly upregulated the mRNA expression of Nrf2 by increase rate ranging from 23% to 50%. However, the low bioavailability of macromolecular active compounds limits their widespread application in cosmetics. To address this issue, various active delivery technologies have been developed, including nanoemulsion technology, encapsulated liposome technology, and microneedles, which effectively enhance penetration [23-24]. Chebulinic acid, despite having the highest enhancement rate, also encountered challenges in penetrating the stratum corneum due to its large molecular weight. Nevertheless, the application of silk fibroin encapsulation technology proved successful in enhancing its transdermal delivery, overcoming the penetration barrier.

This study demonstrates that a virtual screening model combining with appropriate delivery technology, can serve as a helpful tool for identifying potent Keap1-Nrf2 inhibitors. The findings of this study established a method for the discovery of new anti-aging active molecules for skincare applications.

5. References

1. Zhai Y, Dang Y, Gao W, Zhang Y, Xu P, Gu J, Ye X. P38 and JNK signal pathways are involved in the regulation of phlorizin against UVB-induced skin damage. Exp Dermatol. 2015 Apr;24(4):275-9.

2. Lee CW, Ko HH, Chai CY, Chen WT, Lin CC, Yen FL. Effect of Artocarpus communis Extract on UVB Irradiation-Induced Oxidative Stress and Inflammation in Hairless Mice. Int J Mol Sci. 2013 Feb 12;14(2):3860-73.
3. Jakubczyk K, Dec K, Kałduńska J, Kawczuga D, Kochman J, Janda K. Reactive oxygen species - sources, functions, oxidative damage. Pol Merkur Lekarski. 2020 Apr 22;48(284):124-127.
4. Lee CH, Wu SB, Hong CH, Yu HS, Wei YH. Molecular Mechanisms of UV-Induced Apoptosis and Its Effects on Skin Resi-dential Cells: The Implication in UV-Based Phototherapy. Int J Mol Sci. 2013 Mar 20;14(3):6414-35.
5. Hwang E, Park SY, Lee HJ, Lee TY, Sun ZW, Yi TH. Gallic acid regulates skin photoaging in UVB-exposed fibroblast and hairless mice. Phytother Res. 2014 Dec;28(12):1778-88.
6. Fisher GJ, Kang S, Varani J, Bata-Csorgo Z, Wan Y, Datta S, Voorhees JJ. Mechanisms of photoaging and chronological skin aging. Arch Dermatol. 2002 Nov;138(11):1462-70.
7. Mechqoq H, Hourfane S, El Yaagoubi M, El Hamdaoui A, da Silva Almeida JRG, Rocha JM, El Aouad N. Molecular Docking, Tyrosinase, Collagenase, and Elastase Inhibition Activities of Argan By-Products. Cosmetics. 2022; 9(1):24.
8. Itoh K, Wakabayashi N, Katoh Y, Ishii T, Igarashi K, Engel JD, Yamamoto M. Keap1 represses nuclear activation of antiox-idant responsive elements by Nrf2 through binding to the amino-terminal Neh2 domain. Genes Dev. 1999 Jan 1;13(1):76-86.
9. Otake K, Ubukata M, Nagahashi N, Ogawa N, Hantani Y, Hantani R, Adachi T, Nomura A, Yamaguchi K, Maekawa M, Mamada H, Motomura T, Sato M, Harada K. Methyl and Fluorine Effects in Novel Orally Bioavailable Keap1-Nrf2 PPI Inhibitor. ACS Med Chem Lett. 2023 Apr 7;14(5):658-665.
10. Li B, Wang Y, Jiang X, Du H, Shi Y, Xiu M, Liu Y, He J. Natural products targeting Nrf2/ARE signaling pathway in the treatment of inflammatory bowel disease. Biomed Pharmacother. 2023 Aug;164:114950.
11. Montes Diaz G, Hupperts R, Fraussen J, Somers V. Dimethyl fumarate treatment in multiple sclerosis: Recent advances in clinical and immunological studies. Autoimmun Rev. 2018 Dec;17(12):1240-1250.
12. Gorgulla C, Boeszoermenyi A, Wang ZF, Fischer PD, Coote PW, Padmanabha Das KM, Malets YS, Radchenko DS, Moroz YS, Scott DA, Fackeldey K, Hoffmann M, Iavniuk I, Wagner G, Arthanari H. An open-source drug discovery platform enables ultra-large virtual screens. Nature. 2020 Apr;580(7805):663-668.
13. Pallesen JS, Tran KT, Bach A. Non-covalent Small-Molecule Kelch-like ECH-Associated Protein 1-Nuclear Factor Erythroid 2-Related Factor 2 (Keap1-Nrf2) Inhibitors and Their Potential for Targeting Central Nervous System Diseases. J Med Chem. 2018 Sep 27;61(18):8088-8103.
14. Yan C, Zhang Y, Zhang X, Aa J, Wang G, Xie Y. Curcumin regulates endogenous and exogenous metabolism via Nrf2-FXR-LXR pathway in NAFLD mice. Biomed Pharmacother. 2018 Sep;105:274-281.
15. Abdel-Naim AB, Hassanein EHM, Binmahfouz LS, Bagher AM, Hareeri RH, Algandaby MM, Fadladdin YAJ, Aleya L, Abdel-Daim MM. Lycopene attenuates chlorpyrifos-induced hepatotoxicity in rats via activation of Nrf2/HO-1 axis. Ecotoxicol Environ Saf. 2023 Jun 15;262:115122. .
16. Giordano D, Biancaniello C, Argenio MA, Facchiano A. Drug Design by Pharmacophore and Virtual Screening Approach. Pharma-ceuticals (Basel). 2022 May 23;15(5):646.
17. Boyenle ID, Divine UC, Adeyemi R, Ayinde KS, Olaoba OT, Apu C, Du L, Lu Q, Yin X, Adelusi TI. Direct Keap1-kelch inhibitors as potential drug candidates for oxidative stress-orchestrated diseases: A review on In silico perspective. Pharmacol Res. 2021 May;167:105577.

18. Sohilait MR, Pranowo HD, Haryadi W. Molecular docking analysis of curcumin analogues with COX-2. Bioinformation. 2017 Nov 30;13(11):356-359.
19. Wang X, Liu K, Fu S, Wu X, Xiao L, Yang Y, Zhang Z, Lu Q. Silk Nanocarrier with Tunable Size to Improve Transdermal Capacity for Hydrophilic and Hydrophobic Drugs. ACS Appl Bio Mater. 2023 Jan 16;6(1):74-82.
20. Bobasa EM, Phan ADT, Netzel ME, Cozzolino D, Sultanbawa Y. Hydrolysable tannins in Terminalia ferdinandiana Exell fruit powder and comparison of their functional properties from different solvent extracts. Food Chem. 2021 Oct 1;358:129833
21. Babiaka SB, Simoben CV, Abuga KO, Mbah JA, Karpoormath R, Ongarora D, Mugo H, Monya E, Cho-Ngwa F, Sippl W, Loveridge EJ, Ntie-Kang F. Alkaloids with Anti-Onchocercal Activity from Voacanga africana Stapf (Apocynaceae): Identification and Molecular Modeling. Molecules. 2020 Dec 25;26(1):70.
22. Liu P, Tian W, Tao S, Tillotson J, Wijeratne EMK, Gunatilaka AAL, Zhang DD, Chapman E. Non-covalent NRF2 Activation Confers Greater Cellular Protection than Covalent Activation. Cell Chem Biol. 2019 Oct 17;26(10):1427-1435.e5.
23. Kim TG, Lee Y, Kim MS, Lim J. A novel dermal delivery system using natural spicules for cosmetics and therapeutics. J Cosmet Dermatol. 2022 Oct;21(10):4754-4764.
24. Gopi S, Balakrishnan P. Evaluation and clinical comparison studies on liposomal and non-liposomal ascorbic acid (vitamin C) and their enhanced bioavailability. J Liposome Res. 2021 Dec;31(4):356-364.